Title: Abrupt stream acidification and metal mobilization from permafrost degradation

Authors: Elliott K. Skierszkan[1,2*], Andras J. Szeitz[3], Matthew B.J. Lindsay[2], Sean K. Carey[3]

Affiliations:

[1]Department of Earth Science, Carleton University; Ottawa, K1S 5B6, Canada.

[2]Department of Geological Sciences, University of Saskatchewan; Saskatoon, S7N 5E2, Canada.

[3]School of Earth, Environment & Society, McMaster University; Hamilton, L8S 4L8, Canada.

*Corresponding author. ElliottSkierszkan@CUNET.carleton.ca

Abstract

Stream chemistry and ecosystem function are being transformed by abrupt climate-driven acceleration of sulfide-mineral oxidation in permafrost-underlain headwater catchments of the Yukon and Mackenzie river basins—the two largest (sub)Arctic rivers in North America. Over the past decade, dozens of acidic (pH ~3) seepages have emerged in these headwaters, causing vegetation dieback and mobilizing metals at acutely toxic concentrations in receiving streams. Acid generated during sulfide-mineral oxidation also accelerates CO_2 emissions by driving carbonate-mineral dissolution. Major downstream sub(Arctic) rivers show significant multi-decadal sulfate concentration increases, yet their metals concentrations remain stable because of attenuation and dilution processes. Headwater stream acidification signals a major perturbation in metal, carbon, and sulfur cycling linked to permafrost thaw with far-reaching consequences for water resources, northern communities, ecosystem health, and Earth's biogeochemical future.

Large-scale degradation of water quality and enhanced global biogeochemical cycling are being driven by intensified sulfide-mineral oxidation (SMO) associated with permafrost thaw (*1–3*). Permafrost presently underlies >14 million km^2 of land but is disappearing at rates unprecedented over the Holocene Epoch (the last 11,800 years) due to post-industrial climate warming (*4*, *5*). Ground transition toward unfrozen conditions promotes weathering of minerals that have been geochemically dormant for millennia by amplifying mineral-water-microbe interactions (*2*, *6–16*). Sulfide minerals are ubiquitous in sedimentary, igneous, and metamorphic rocks, and their oxidative weathering liberates acidity, sulfate, and metals to water (*17*). SMO also modulates global climate by producing acid that drives carbonate mineral dissolution and CO_2 production (*18*). SMO can lead to acid-rock drainage (ARD), a condition characterized by acidic water with toxic metal and metalloid (hereafter referred to as metals) concentrations (*17*, *19*, *20*). Waterbodies receiving ARD are characteristically discolored by ocherous and white precipitates associated with secondary-mineral precipitation (*21*). Intensified SMO from permafrost degradation may profoundly alter biogeochemical cycles with global implications for water resources, aquatic ecosystems, and Earth's climate.

Intensified SMO in permafrost regions is evidenced by significant increases in sulfate concentrations and fluxes in recent decades in the Mackenzie and Yukon river basins, which contribute ~20% of riverine discharge to the Arctic Ocean (*3*, *22*). Localized ARD related to permafrost thaw and deglaciation has also been observed in headwater catchments of the Andes, the Pyrenees, the Alps, and Alaska's Brooks Range, resulting in devastation of aquatic macroinvertebrate and fish communities and "rusting" of streams (*1*, *23–26*). Understanding the breadth, timing, and mechanisms of SMO acceleration in thawing permafrost requires observations linking large river basins, where solute concentrations are modulated by dilution and attenuation processes, with smaller headwater catchments where SMO signals are most clearly manifested, and biological impacts most acute. Hydrological and geochemical records in headwater catchments may therefore reveal the timing and mechanisms of SMO intensification not captured by the large rivers, and provide mechanistic insights into a globally significant yet underappreciated permafrost-climate feedback.

Here, we describe abrupt ARD onset in small (<40 km^2) permafrost-underlain headwater catchments of the Yukon and Mackenzie river basins. Our hydrological and geochemical dataset captures precipitous declines in water quality towards highly acidic levels (pH <4) and acutely toxic metals concentrations within a <5 year period. We further link this trend to broader regional acceleration of SMO in receiving rivers of the Yukon and Mackenzie basins. Thawing permafrost-underlain headwater catchments emerge as biogeochemical reactors that drive export of metals, sulfur, and carbon back into active hydrological and biogeochemical cycles, unveiling a growing environmental risk in a warming cryosphere.

Accelerating SMO reshapes water quality and ecosystems along the Yukon-Mackenzie divide

Our detailed time-series observations come from three headwater catchments (11 to 36 km^2) in the Tombstone Waters Observatory (TWO) in central Yukon, Canada, a high-latitude (~64 to 65°N) observatory straddling the Yukon-Mackenzie watershed divide (fig. S1). These catchments are unimpacted by local anthropogenic disturbances (e.g., mining). The nearest long-term temperature records show a 0.4°C increase per decade since 1961 (fig. S2), translating to greater local permafrost degradation now than at any time over the Holocene Epoch (*27*). TWO catchments, approximately located at kilometer markers KM71, KM99, and KM175 along the Dempster Highway in Yukon, overlie marine sedimentary rocks deposited offshore of Laurentia, the ancient North American craton (fig. S1). Sulfide-rich black-shales capable of producing ARD commonly occur within these sedimentary rocks (*1*, *3*, *28*). KM99 and KM175 streams feed the Ogilvie (~5,410 km^2) and Peel (~74,000 km^2) rivers in the Mackenzie River basin. KM71 stream feeds the Yukon River via the Klondike (~7,800 km^2) River. Multidecadal chemistry datasets for these downstream (sub)Arctic rivers help link recent evolution in TWO headwater stream chemistry to broader subcontinental-scale shifts in weathering regimes.

The Peel River basin shows widespread impact from SMO. Satellite-image analyses from August 2024 reveal 146 affected stream reaches across ~59,500 km^2 (Fig. 1A). Stream discoloration extended hundreds of meters to tens of kilometers downstream of ARD inputs (Fig. 1A). A large proportion of impacted streams have relatively small catchment areas, with 121 streams draining <100 km^2, 22 streams draining 100 – 500 km^2, and three streams draining >500 km^2. Geology is a key ARD driver in this region, particularly in catchments underlain by fine-grained siliciclastic-dominated geology (e.g., shale, siltstone) (Fig. 1A). In contrast, ARD is limited in carbonate-dominated catchments

Geochemical monitoring in headwater streams reveals abrupt degradation of water quality linked to SMO, especially since 2024. The poorest water quality we observed among headwater streams was in a 63 km^2 subcatchment of the Ogilvie River (KM228) that in 2000 had circumneutral pH with <100 mg L^{-1} sulfate (*29*). KM228 stream experienced considerable riparian thermokarst between 2007 and 2025 (fig. S3B-C). By July 2025, its pH was 3.3, with extreme concentrations of sulfate (10,800 mg L^{-1}) and dissolved metals (operationally defined here as passing a <0.45 µm filter) including iron (670 mg L^{-1}), aluminium (68 mg L^{-1}), zinc (33 mg L^{-1}), and cadmium (13 mg L^{-1}). It produced a plume of metalliferous precipitate visible up to 3 km downstream of its confluence with the Ogilvie River (fig. S3A).

Field observations and remote-sensing analyses in the Peel and Klondike river basins also reveal pervasive vegetation dieback—patches of vegetation killed by emergent acidic seepages—up to 90,350 m^2 in area appearing within the last decade (Fig. 1B-C, Fig. 2B-C, fig. S4). Similar diebacks were

recently reported in the Alaskan Brooks Range, suggesting a more widespread phenomenon in the western North American Arctic (*1*). Dieback commonly originates along hillslopes and contains oxic seepages (fig. S4, table S1), suggesting that acid generation may be promoted where topography drives infiltration of oxygenated water into a deepening sulfide-bearing active-layer. Active-layer seepages within dieback areas were highly acidic with a median pH of 3.1 (n=10), up to 17,610 mg L^{-1} sulfate, and specific conductivity of up to 13,890 µS cm^{-1} (table S1). Their metals concentrations were also extreme, reaching 1,277 mg L^{-1} aluminium, 499 mg L^{-1} zinc, 318 mg L^{-1} iron, 88 mg L^{-1} manganese, 64 mg L^{-1} nickel, and 6.0 mg L^{-1} cadmium (table S2). These concentrations are comparable to those observed in effluents from some of the world's most contaminated mine sites (*30*), surpassing acute toxicity thresholds for most terrestrial and aquatic organisms by several orders of magnitude. Soils within vegetation diebacks harbor secondary sulfate mineral precipitates (gypsum, epsomite, pickeringite, tamarugite, scapolite) formed by evapoconcentration and which temporarily store sulfate and metals that can be flushed during rainfall and snowmelt (fig. S5A) (*17*).

Abrupt stream acidification over the last decade

Vegetation diebacks reveal ARD point-sources that degrade water quality in receiving streams. This effect is evident in KM99 stream, where vegetation dieback first appeared circa 2015 and has expanded to ~1,900 m^2 in summer 2024 (Fig. 1C and Fig. 2B). The dieback comprises only ~0.02% of the stream catchment area, yet completely dominates downstream water chemistry. Active-layer seepage in the dieback had pH of 2.7, with elevated sulfate (4,924 mg L^{-1}), zinc (499 mg L^{-1}), aluminium (303 mg L^{-1}), manganese (88 mg L^{-1}), nickel (62 mg L^{-1}), cadmium (5.1 mg L^{-1}), and other metals (table S1). Stream pH decreased from 8.0 upstream of the dieback to 5.8 immediately downstream, coincident with a ~3 orders-of-magnitude increase in sulfate and metals concentrations (fig. S6). pH buffering in the lower reach of the stream, attributed to carbonate-dominated geology, led to a pH increase back to circumneutral values (pH 6.7 ± 1.0). This pH buffering, evidenced by measurable alkalinity at the stream outlet (fig. S7), drives extensive formation of milky-white and ocherous red precipitates that have discolored streamwater (Fig. 1A) and coated the streambed downstream of the dieback since 2023 (fig. S5B).

Mineralogical analyses indicated that these precipitates were composed of metal-(oxyhydroxy)sulfates commonly associated with ARD and effluents emanating from sulfide-rich mine wastes (*21*). Within acidic seepages at pH ~3, they comprised suspended aluminum-iron phases with elevated nickel and zinc, and chemistry and morphology diagnostic of schwertmannite (fig. S8E-F) (*31*). Further downstream and at pH ~6, suspended particles were composed of aluminum and sulfur, typical of phases precipitating during ARD neutralization (*21*, *32*) (fig. S8C-D). At the stream outlet where pH was circumneutral, precipitates were composed of aluminum and iron with variable sulfur, nickel, and zinc contents (fig.

S8A-B). These downstream precipitates are interpreted as nanocrystalline to amorphous aluminum- and iron-(oxyhydr)oxides or hydroxysulfates (*33*), consistent with streamwater saturation with respect to these phases (fig. S9). Geochemical modeling suggests that conditions can be favorable to gypsum and jarosite precipitation near pH ~3 seepages, while conditions favorable to carbonate precipitation (rhodochrosite [$MnCO_3$] and smithsonite [$ZnCO_3$]) may develop as downstream pH increases (fig. S9). These mineralogically diverse precipitates modulate metal transport downstream of acidic seepages. Their stability is controlled by factors such as pH and water chemistry that vary spatially, which creates uncertainty regarding their overall role as metal sinks or sources.

Interannual high-frequency geochemical time-series of TWO streams captured a precipitous decline in water quality in 2023-2025. In KM99 stream, visible water discoloration began in summer 2023 and pH has been significantly lower since that time, while sulfate and metals (cadmium, cobalt, manganese, nickel, selenium, zinc) have increased by orders of magnitude compared (fig. S10). The most pronounced water quality degradation occurred in KM175 stream beginning in 2025. This stream pH was historically circumneutral (e.g., pH 7.5 ± 0.3 in 2019-2022), yet reached values as low as 2.7 in 2025, with a mean 2025 pH of 5.0 ± 1.5 (Fig. 2). This pH decrease drove major increases in sulfate, and the stream's concentrations (aluminum, arsenic, cobalt, cadmium, copper, iron, manganese, nickel, selenium and zinc) now exceed acute toxicity thresholds for aquatic organisms (table S2). KM175 streamwater was also turbid because of suspended metal precipitates (Fig. 1A). Like KM99 stream, multiple vegetation diebacks over shale bedrock also occur within KM175 catchment and contained pH ~3 seepages with extreme sulfate and metals concentrations (Fig. 2C, fig. S4C-D, and table S1). Temporal degradation of water quality at KM71 stream followed similar trends to those observed in KM99 and KM175 streams, but it was more subdued due to the stream's higher alkalinity that buffers pH (fig. S7 and fig. S11). Metals concentrations in all three TWO streams now routinely exceeded Canadian guidelines for the protection of aquatic life (*34*) with respect to multiple metals (table S2). Their pH and sulfate concentrations were all significantly higher in 2024-2025 relative to earlier years (fig. S12). These abrupt geochemical transitions echo patterns typical of sulfide-rich mine waste impoundments when acid-buffering capacity is depleted and runaway SMO leads to ARD (*17*).

Major interannual shifts in stream specific conductivity-discharge relationships further capture the step-change in stream chemical regimes over the last 3 years (Fig. 3). Under steady-state hydrogeochemical conditions, specific conductivity typically peaks during periods of low-discharge, when longer residence times promote greater water-mineral interaction, while it is low during periods of high discharge because of dilution by rainfall and snowmelt runoff (*15*, *35*). Interannual records show that these predictable seasonal relationships have become overprinted by a larger interannual shift beginning in 2023 at KM99

and in 2024 at KM175 stream, when specific conductivity values began increasing outside of prior year values over the range of discharges (Fig. 3). High specific conductivity values reflect increased solute loads as dissolved SMO products are mobilized into stream networks.

Sulfate, metal, and carbon fluxes linked to intensified sulfide-mineral oxidation

Sulfate fluxes computed from continuous discharge-concentration relationships generally scale with cumulative water discharges (fig. S13 and table S3). However, apparent deviations from this trend occurred in 2024 and 2025, reflecting recent SMO intensification. Mean daily sulfate fluxes computed from concentration-discharge relationships during summer months ranged from 0.43 ± 0.24 kmol km^{-2} d^{-1} in KM99 stream to 2.2 ± 0.4 kmol km^{-2} d^{-1} in KM175 stream (table S4). Using average nickel/sulfate and zinc/sulfate ratios in pH <3.2 acidic seepages, where nickel and zinc precipitation and sorption reactions are minimized (*17*), we estimated that 20 ± 4 kg zinc km^{-2} d^{-1} and 4.0 ± 2.2 kg nickel m^{-2} d^{-1} were mobilized in the KM175 catchment (table S4). It is important to highlight that metal fluxes likely represent a localized upper bound, because metal export is attenuated between point-sources of ARD and receiving waterbodies as increasing pH drives sorption and secondary mineral precipitation reactions and decreases the metal/sulfate ratio (Fig. 4D).

Stoichiometric calcium+magnesium vs. sulfate relationships were indicative of dissolution of carbonate minerals by sulfuric acid attack in TWO streams (fig. S14). Inputs from marine evaporite dissolution (e.g., gypsum, $CaSO_4•2H_2O$) can be ruled out based on sulfur and oxygen isotope analyses of streamwater sulfate (table S5) (*36*). Using calcium and magnesium fluxes to estimate daily inorganic carbon fluxes yielded values ranging from 8.2 ± 3.9 kg km^{-2} in KM99 stream up to 110 ± 29 kg km^{-2} in KM175 stream. Given that the acidic pH of KM175 stream drives inorganic carbon speciation towards CO_2, this catchment alone could be emitting as much as 403 ± 105 kg CO_2 km^{-2} daily. Over the 35.9 km^2 stream basin, this translates to ~14.5 t CO_2 d^{-1}, which is equivalent to the daily anthropogenic emissions of ~1,120 people using global average emission estimates (*37*). These results suggest that SMO intensification in headwater basins not only constitutes an environmental water-quality crisis for receiving aquatic ecosystems, but also contributes considerable greenhouse gas emissions in the form of CO_2 (*3*, *38*).

Rapid recent increases in tributary river sulfate concentrations from intensified SMO

SMO intensification in Yukon and Mackenzie headwater catchments is consistent with interdecadal increases in sulfate concentrations in downstream tributary rivers (Fig. 4). Sulfate concentration time-series for the undisturbed Ogilvie and Peel rivers indicate that this phenomenon arises through climate-driven processes. Similar mechanisms likely drive interdecadal trends in the Klondike River. Additional

sulfate inputs associated with placer mining in the Klondike basin might be possible, but are likely limited because of the low sulfide content of local placer deposits. Moreover, sulfate concentrations are rising at increasing rates in all three rivers (Fig. 4). Peel River sulfate concentrations increased at a rate of +2.1 mg L^{-1} yr^{-1} from 2000-2025, which is double the rate observed from 1979-2000. Although the Ogilvie and Klondike River records contain gaps between the late 1990s and the early 2000s, sulfate concentrations in the 2000s increased at rates of +12 mg L^{-1} yr^{-1} and +1.6 mg L^{-1} yr^{-1}, respectively. In contrast, in the late 1990s these rates were marginally significant for the Ogilvie ($p=0.04$) and non-significant for the Klondike ($p=0.97$). Rapidly rising rates of sulfate export, particularly over the last 10 years, underscore subcontinental-scale SMO acceleration (*3*, *22*).

Despite these added acid inputs, pH remains alkaline and stable in the large and well-mixed downstream rivers (Klondike: 7.9 ± 0.2, Ogilvie: 8.1 ± 0.2, and Peel: 7.9 ± 0.4) reflecting substantial within-catchment buffering. Riverine filter-passing and total metals (aluminum, iron, manganese, nickel, and zinc) exhibit no clear interannual trends, in contrast with sulfate (fig. S15). The decoupling of metal and sulfate trends in major rivers indicates metal attenuation between ARD point sources and receiving waterbodies through pH-driven precipitation and sedimentation processes. Metal attenuation processes across spatial scales are further revealed through pH-driven decreases in metal/sulfate ratios from ARD-impacted headwater catchments to receiving tributaries (Fig. 4D). While metal transport from headwaters is partly attenuated by precipitation, sorption, and sedimentation along flowpaths and river networks, these secondary reactions do not eliminate ecological risk. Most of the secondary minerals observed are metastable, and their stability depends on evolving geochemical conditions in streams, rivers, and sedimentation areas. Metastable metal-rich precipitates also accumulate in depositional environments, coating streambeds, stressing benthic habitats (*1*), and could create long-term ecological hazards as they recrystallize or dissolve.

Environmental implications of intensified sulfide-mineral oxidation in permafrost catchments

By linking headwater processes with multi-decadal river chemistry records (*1*, *3*, *22–24*), our multiscale analysis closes a critical knowledge gap and reveals rapid, widespread SMO intensification, associated vegetation dieback, and sulfate and metal mobilization across the western North American (sub)Arctic. At larger scales, enhanced export of micronutrients such as iron and zinc, two metals characteristic of ARD and growth-limiting nutrients in the pelagic oceans (*39*), could alter ocean productivity, even as acidification and metal toxicity degrade headwater ecosystems. These findings elevate SMO from a local geomorphic process to a larger biogeochemical risk, with cascading consequences for aquatic ecosystems, northern communities, mineral exploration, and global climate.

Accelerated SMO in Yukon and Alaska arises from the intersection of permafrost thaw with sulfide-rich sedimentary terranes including the North American basin and platform and Arctic Alaska terranes that formed offshore Laurentia (fig. S16) (*1*, *25*, *28*, *40*, *41*). Largescale historical (1976-2001) synoptic stream pH surveys in Yukon reveals that 2% of streams overlying these terranes have pH <5—a percentage forty times higher than other geological terranes of western Cordillera in Yukon. These sedimentary terranes are primed for ARD generation as sulfide weathering intensifies (fig. S16). They cumulatively underlie more than 1.1 million km^2 of western North America's permafrost zone—extending from northern Alaska through Yukon Territory and the Northwest Territories. However, subcontinental-scale ARD vulnerability depends on local acid-generating and buffering capacity, which ultimately is driven by sulfide/carbonate ratios. Not all siliciclastic strata are sulfide-rich, and they are also often proximal to carbonate-bearing strata (Fig. 1). Carbonates can buffer acidity and improve water quality, but in so doing drive CO_2 release through carbonate dissolution (*3*). Even under well-buffered conditions, certain hazardous metals remain mobile (e.g., arsenic, nickel, selenium, uranium) (*42*). Constraining ARD vulnerability within this vast region will require refined geological, mineralogical, and geochemical mapping, enhanced remote-sensing, and updated hydrochemical monitoring. Once initiated, ARD can persist for millennia (*43*). Importantly, intensified sulfur cycling of similar magnitude accompanied the last major global climatic transition at the Pleistocene–Holocene boundary (*44*). A comparable disruption appears to be unfolding in the modern warming (sub)Arctic.

References and Notes

1. J. A. O'Donnell, M. P. Carey, J. C. Koch, C. Baughman, K. Hill, C. E. Zimmerman, P. F. Sullivan, R. Dial, T. Lyons, D. J. Cooper, B. A. Poulin, Metal mobilization from thawing permafrost to aquatic ecosystems is driving rusting of Arctic streams. *Communications Earth & Environment* **5,** 268 (2024).

2. E. K. Skierszkan, J. W. Dockrey, M. B. J. Lindsay, Enhanced metal mobilization from thawing permafrost is an emergent risk to water resources. *Environmental Science & Technology - Water* **5**, 20–32 (2024).

3. E. V. Walsh, R. G. Hilton, S. E. Tank, E. Amos, Temperature sensitivity of the mineral permafrost feedback at the continental scale. *Science Advances* **10**, eadq4893 (2024).

4. J. Obu, S. Westermann, A. Bartsch, N. Berdnikov, H. H. Christiansen, A. Dashtseren, R. Delaloye, B. Elberling, B. Etzelmüller, A. Kholodov, A. Khomutov, A. Kääb, M. O. Leibman, A. G. Lewkowicz, S. K. Panda, V. Romanovsky, R. G. Way, A. Westergaard-Nielsen, T. Wu, J. Yamkhin, D. Zou, Northern Hemisphere permafrost map based on TTOP modelling for 2000–2016 at 1 km^2 scale. *Earth-Science Reviews* **193**, 299–316 (2019).

5. Intergovernmental Panel on Climate Change, *Climate Change 2013 - Working Group 1 Contribution to the Fifth Assessment Report of the Intergovernmental Panel on Climate Change*, (Intergovernmental Panel on Climate Change, 2013).

6. A. J. Barker, T. D. Sullivan, W. B. Baxter, R. A. Barbato, S. Gallaher, G. E. Patton, J. P. Smith, T. A. Douglas, Iron oxidation-reduction processes in warming permafrost soils and surface waters expose a seasonally rusting Arctic watershed. *ACS Earth and Space Chemistry* **7**, 1479–1495 (2022).

7. M. S. Patzner, C. W. Mueller, M. Malusova, M. Baur, V. Nikeleit, T. Scholten, C. Hoeschen, J. M. Byrne, T. Borch, A. Kappler, C. Bryce, Iron mineral dissolution releases iron and associated organic carbon during permafrost thaw. *Nature Communications* **11**, 1–11 (2020).

8. M. S. Patzner, N. Kainz, E. Lundin, M. Barczok, C. Smith, E. Herndon, L. Kinsman-Costello, S. Fischer, D. Straub, S. Kleindienst, A. Kappler, C. Bryce, Seasonal fluctuations in iron cycling in thawing permafrost peatlands. *Environmental Science & Technology* **56**, 4620–4631 (2022).

9. E. Herndon, L. Kinsman-Costello, S. Godsey, "Biogeochemical cycling of redox-sensitive elements in permafrost-affected ecosystems" in *Biogeochemical Cycles: Ecological Drivers and Environmental Impact*, K. Donstova, Z. Balogh-Brunstad, G. Le Roux, Eds. (American Geophysical Union and John Wiley & Sons, Inc., ed. 1, 2020), pp. 254–266.

10. O. S. Pokrovsky, R. M. Manasypov, A. V. Chupakov, S. Kopysov, Element transport in the Taz River, western Siberia. *Chemical Geology* **614**, 121180 (2022).

11. O. S. Pokrovsky, R. M. Manasypov, S. V. Loiko, L. S. Shirokova, Organic and organo-mineral colloids in discontinuous permafrost zone. *Geochimica et Cosmochimica Acta* **188**, 1–20 (2016).

12. O. S. Pokrovsky, M. Bueno, R. M. Manasypov, L. S. Shirokova, J. Karlsson, D. Amouroux, Dissolved organic matter controls seasonal and spatial selenium concentration variability in thaw lakes across a permafrost gradient. *Environmental Science & Technology* **52**, 10254–10262 (2018).

13. C. R. Burn, A. Bartsch, E. Chakraborty, S. Das, R. Frauenfelder, I. Gärtner-Roer, K. G. Gisnås, T. Herring, B. J. Jones, S. V. Kokelj, E. Lathrop, J. B. Murton, D. M. Nielsen, F. Niu, C. Olson, B. H. O'Neill, S. Opfergelt, P. P. Overduin, K. Schaefer, E. A. G. Schurr, E. K. Skierszkan, S. L. Smith, S. M. Stuenzi, S. E. Tank, G. Vieira, S. Westernann, S. A. Wolfe, E. Yarmak, Developments in permafrost science and engineering in response to climate warming in

circumpolar and high mountain regions, 2019-2024. *Permafrost and Periglacial Processes* **36**, 167-188 (2024).

14. E. K. Skierszkan, V. A. Schoepfer, M. D. Fellwock, M. B. J. Lindsay, Uranium speciation and mobilization in thawing permafrost. *Environmental Science & Technology* **58**, 17058–17069 (2024).

15. E. K. Skierszkan, S. K. Carey, S. I. Jackson, M. Fellwock, C. Fraser, M. B. J. Lindsay, Seasonal controls on stream metal(loid) signatures in mountainous discontinuous permafrost. *Science of the Total Environment* **908**, 167999 (2024).

16. E. K. Skierszkan, V. A. Schoepfer, M. D. Fellwock, A. Hayatifar, V. F. Bondici, J. M. McBeth, J. W. Dockrey, M. B. J. Lindsay, Arsenic mobilization induced by thawing permafrost. *Earth and Space Chemistry* **8**, 745–759 (2024).

17. D. W. Blowes, C. J. Ptacek, J. L. Jambor, C. G. Weisener, D. Paktunc, W. D. Gould, D. B. Johnson, *The Geochemistry of Acid Mine Drainage* (Elsevier Ltd., ed. 2, 2013).

18. M. A. Torres, N. Moosdorf, J. Hartmann, J. F. Adkins, A. J. West, Glacial weathering, sulfide oxidation, and global carbon cycle feedbacks. *Proceedings of the National Academy of Sciences U.S.A.* **114**, 8716–8721 (2017).

19. M. B. J. Lindsay, M. C. Moncur, J. G. Bain, J. L. Jambor, C. J. Ptacek, D. W. Blowes, Geochemical and mineralogical aspects of sulfide mine tailings. *Applied Geochemistry* **57**, 157–177 (2015).

20. D. K. Nordstrom, C. N. Alpers, "Geochemistry of acid mine waters" in *The Environmental Geochemistry of Mineral Deposits: Part A: Processes, Techniques, and Health Issues Part B: Case Studies and Research Topics,* G. S. Plumlee, M. J. Logsdon, L. F. Filipek, Eds. (Society of Economic Geologists, 1997), pp. 133–160.

21. D. K. Nordstrom, Geochemical modeling of iron and aluminum precipitation during mixing and neutralization of acid mine drainage. *Minerals* **10**, 1–12 (2020).

22. R. C. Toohey, N. M. Herman-Mercer, P. F. Schuster, E. A. Mutter, J. C. Koch, Multidecadal increases in the Yukon River Basin of chemical fluxes as indicators of changing flowpaths, groundwater, and permafrost. *Geophysical Research Letters* **43**, 12,120–12,130 (2016).

23. M. Zarroca, C. Roqué, R. Linares, J. G. Salminci, F. Gutiérrez, Natural acid rock drainage in alpine catchments: A side effect of climate warming. *Science of the Total Environment* **778**, 146070 (2021).

24. C. Wanner, H. Moradi, P. Ingold, M. A. Cardenas Bocanegra, R. Mercurio, G. Furrer, Rock glaciers in the Central Eastern Alps – How permafrost degradation can cause acid rock drainage, mobilization of toxic elements and formation of basaluminite. *Global and Planetary Change* **227**, 104180 (2023).

25. P. F. Sullivan, R. J. Dial, D. J. Cooper, C. Diamond, C. J. Tino, D. D. Gregory, R. E. Wong, T. W. Lyons, Wild, scenic, and toxic: Recent degradation of an iconic Arctic watershed with permafrost thaw. *Proceedings of the National Academy of Sciences U.S.A.* **122**, e2425644122 (2025).

26. J. L. Garcia, Y. E. Huaman-Navarro, B. L. Willems, R. Loayza-Muro, P. Moreira-Turqu, J. L. Wadham, M. L. Macdonald, A. Bustamante, Identifying acid lakes and associated rock exposure in glacial retreat zones in the Peruvian Andes using Landsat 8 imagery. *Environmental Monitoring and Assessment* **197**, 532 (2025).

27. T. J. Porter, S. W. Schoenemann, L. J. Davies, E. J. Steig, S. Bandara, D. G. Froese, Recent summer warming in northwestern Canada exceeds the Holocene thermal maximum. *Nature Communications* **10**, 1–10 (2019).

28. Y. T. J. Kwong, G. Whitley, P. Roach, Natural acid rock drainage associated with black shale in the Yukon Territory, Canada. *Applied Geochemistry* **24**, 221–231 (2009).

29. D. Héon, Stream sediment analysis, Yukon Regional Geochemical Database, (2003); https://data.geology.gov.yk.ca/Reference/42232.

30. Z. Bao, J. Bain, S. P. Holland, D. Wilson, C. J. Ptacek, D. W. Blowes, Hydrogeochemical response of a variably saturated sulfide-bearing mine waste-rock pile to precipitation: A field-scale study in the discontinuous permafrost region of northern Canada. *Water Resources Research* **58**, e2021WR031082 (2022).

31. V. A. Schoepfer, E. D. Burton, Schwertmannite: A review of its occurrence, formation, structure, stability and interactions with oxyanions. *Earth-Science Reviews* **221**, 103811 (2021).

32. E. K. Skierszkan, J. S. Stockwell, J. W. Dockrey, D. Weis, R. D. Beckie, K. U. Mayer, Molybdenum (Mo) stable isotopic variations as indicators of Mo attenuation in mine waste-rock drainage. *Applied Geochemistry* **87**, 71–83 (2017).

33. S. Carrero, A. Fernandez-Martinez, R. Pérez-López, J. M. Nieto, Basaluminite structure and its environmental implications. *Procedia Earth and Planetary Science* **17**, 237–240 (2017).

34. Canadian Council of Ministers of the Environment, "Canadian water quality guidelines for the protection of aquatic life: Uranium" in *Canadian Environmental Quality Guidelines* (Canadian Council of Ministers of the Environment, 1999), pp. 1–9.

35. S. E. Godsey, J. W. Kirchner, D. W. Clow, Concentration-discharge relationships affect chemostatic characteristics of US catchments. *Hydrological Processes* **23**, 1844–1864 (2009).

36. D. R. Van Stempvoort, J. Spoelstra, G. Bickerton, G. Koehler, B. Mayer, M. Nightingale, J. Miller, Sulfate in streams and groundwater in a cold region (Yukon Territory, Canada): Evidence of weathering processes in a changing climate. *Chemical Geology* **631**, 121510 (2023).

37. H. Ritchie, P. Rosado, M. Roser, Data Page: CO_2 emissions per capita, *Our World in Data. https://ourworldindata.org/grapher/co-emissions-per-capita* (2024).

38. P. C. Kemeny, G. K. Li, M. Douglas, W. Berelson, A. J. Chadwick, N. F. Dalleska, M. P. Lamb, W. Larsen, J. S. Magyar, N. E. Rollins, J. Rowland, M. I. Smith, M. A. Torres, S. M. Webb, W. W. Fischer, A. J. West, Arctic permafrost thawing enhances sulfide oxidation. *Global Biogeochemical Cycles* **37**, 1–36 (2023).

39. J. Duan, R. Cloete, J. C. Loock, A. Lanzirotti, M. Newville, A. Martínez-García, D. M. Sigman, P. J. Lam, A. N. Roychoudhury, S. C. B Myneni, Biogenic-to-lithogenic handoff of particulate Zn affects the Zn cycle in the Southern Ocean. *Science* **384***,* 1235–1240 (2024).

40. D. Lacelle, R. Léveillé, Acid drainage generation and associated Ca-Fe-SO4 minerals in a periglacial environment, Eagle Plains, Northern Yukon, Canada: A potential analogue for low-temperature sulfate formation on Mars. *Planetary and Space Science* **58**, 509–521 (2010).

41. M. Colpron, J. A. L. Nelson, D. C. Murphy, Northern Cordilleran terranes and their interactions through time. *GSA Today* **17**, 4–10 (2007).

42. B. Vriens, E. K. Skierszkan, M. St-Arnault, K. Salzsauler, C. Aranda, K. U. Mayer, R. D. Beckie, Mobilization of metal(oid) oxyanions through circumneutral mine waste-rock drainage. *ACS Omega* **4**, 10205–10215 (2019).

43. J. S. España, E. L. Pamo, E. Santofimia, O. Aduvire, J. Reyes, D. Barettino, Acid mine drainage in the Iberian Pyrite Belt (Odiel river watershed, Huelva, SW Spain): Geochemistry, mineralogy and environmental implications. *Applied Geochemistry* **20**, 1320–1356 (2005).

44. R. E. Stevens, H. Reade, K. L. Sayle, J. A. Tripp, D. Frémondeau, A. Lister, I. Barnes, M. Germonpré, M. Street, J. B. Murton, S. H. Bottrell, D. H. James, T. F. G. Higham, Major excursions in sulfur isotopes linked to permafrost change in Eurasia during the last 50,000 years. *Nature Geoscience* **18**, 961–965 (2025).

45. The dataset for the study may be found at DOI: 10.5061/dryad.cnp5hqcj0.

46. Government of Canada - Environment and Climate Change Canada, National Long-Term Water Quality Monitoring Data. https://open.canada.ca/data/en/dataset/67b44816-9764-4609-ace1-68dc1764e9ea. Consulted June 17, 2025. (2025).

47. D. L. Parkhurst, C. A. J. Appelo, PHREEQC version 3 – A computer program for speciation, batch-reaction, one-dimensional transport, and inverse geochemical calculations. U.S. Geological Survey Techniques and Methods Book 6, Chapter A43, 497p. (2013). https://water.usgs.gov/water-20 resources/software/PHREEQC/index.html.

48. P. E. Reiller, M. Descostes, Development and application of the thermodynamic database PRODATA dedicated to the monitoring of mining activities from exploration to remediation. *Chemosphere* **251,** 126301 (2020).

49. C. A. Schneider, W. S. Rasband, K. W. Eliceiri, NIH Image to ImageJ: 25 years of image analysis. *Nature Methods* **9**, 671–675 (2012).

50. S. Huang, L. Tang, J. P. Hupy, Y. Wang, G. Shao, A commentary review on the use of normalized difference vegetation index (NDVI) in the era of popular remote sensing. *Journal of Forestry Research* **32**, 1–6 (2021).

Acknowledgements

We are grateful to Dr. Arsh Grewal, Dr. Erin Nicholls, Calvin Newbery, Amanda Harrison, Natalie de Freitas, Hayden Ivie, Rosy Tutton, Tyler de Jong, and David Barrett for their involvement in sample collection and efforts towards establishing the Tombstone Waters Observatory. We thank Dr. Jing Chen, Dr. Valerie Schoepfer, Stu Ferry, and Ariel Panozo-Cabrera at the University of Saskatchewan's Environmental Geochemistry Laboratory for assistance with geochemical and mineralogical analyses and sample handling. We thank Rosie Cobbett and Panya Lipovsky with the Yukon Geological Survey for providing photographs of the acidic seepages in the study catchment KM71. The study area overlies traditional territory of the Tr'ondëk Hwëch'in and the First Nation of Na-Cho Nyäk Dun.

Funding:

Natural Sciences and Engineering Research Council of Canada, Discovery Grant RGPIN-2020-06722 (SKC)

Natural Sciences and Engineering Research Council of Canada, Discovery Grant RGPIN-2020-05172 (MBJL)

Natural Sciences and Engineering Research Council of Canada, Discovery Grant RGPIN-2025-04676 (EKS)

Natural Sciences and Engineering Research Council of Canada, Banting Postdoctoral Fellowship (EKS)

Natural Sciences and Engineering Research Council of Canada, Canada Graduate Scholarship – Doctoral (AJS)

Global Water Futures and Global Water Futures Observatory Programs, under the Canada First Excellence Research Fund and CFI-MSI program (SKC, MBJL)

Canada Water Agency GCXE26A074 (SKC, EKS)

Author contributions: All authors contributed to conceptualization, methodology, investigation, visualization, project administration, funding acquisition, and writing (original draft, review & editing). Supervision was performed by SKC and MBJL.

Competing interests:

Authors declare that they have no competing interests.

Data and materials availability:

Original data associated with this manuscript are hosted at Dryad DOI: 10.5061/dryad.cnp5hqcj0 (*45*). Stream water and acidic seepage chemistry data are provided in the Supplementary Materials. River chemistry datasets for the Klondike, Peel, and Ogilvie rivers are available through Environment and Climate Change Canada's National Long-Term Water Quality Monitoring Data (https://open.canada.ca/data/en/dataset/67b44816-9764-4609-ace1-68dc1764e9ea).

No new materials were generated for this study.

Supplementary Materials

Materials and Methods
Figs. S1 to S16
Tables S1 to S5
References (*46-50*)

Figures and Captions

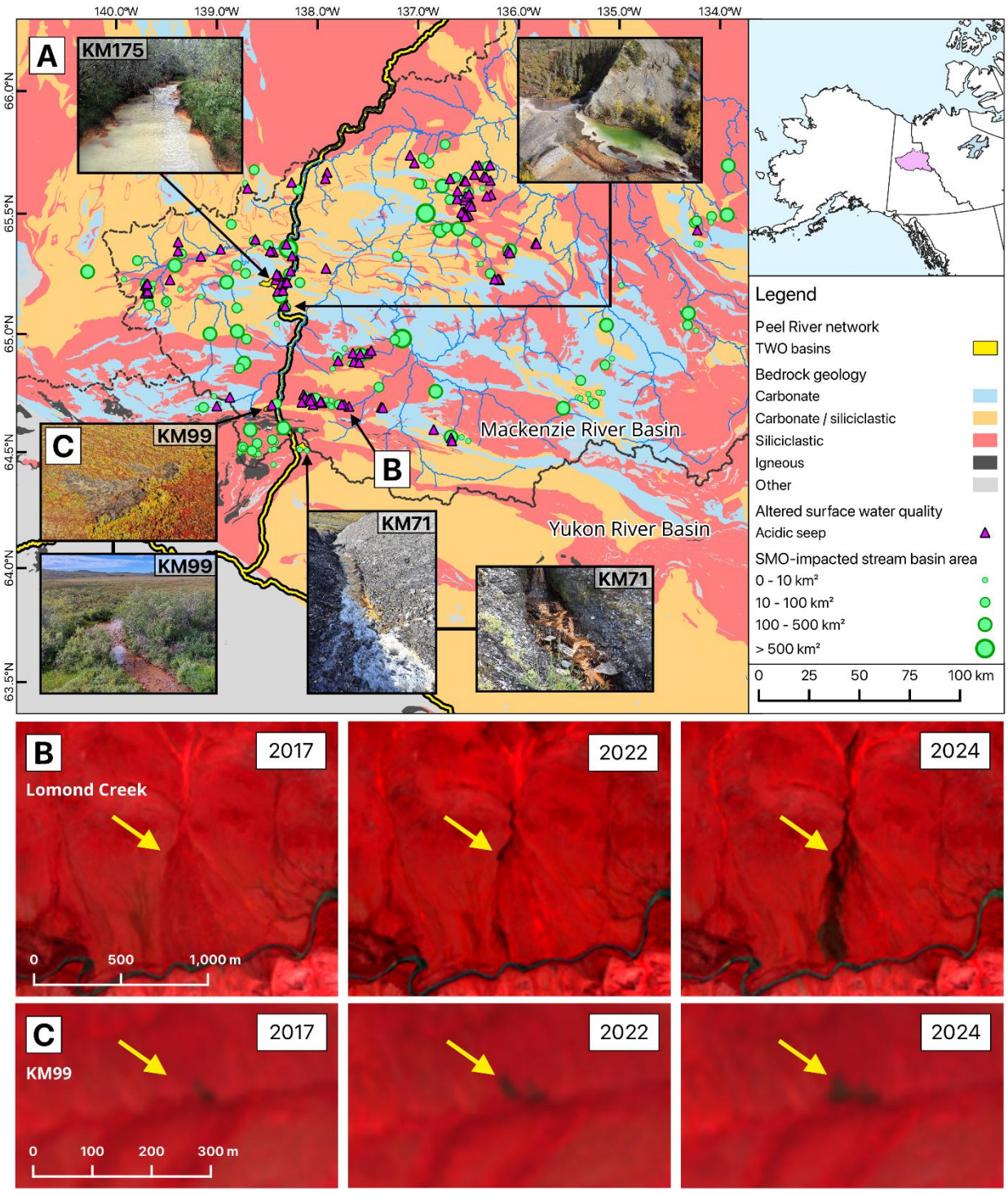

Fig. 1. Regional compilation of acidic seepages, vegetation dieback, and SMO-impacted streams in Peel and Klondike watersheds. (**A**) Widespread SMO-impacted basins, acidic seeps, and vegetation dieback, particularly in fine-grained siliciclastic rocks and rarely in carbonate-dominated catchments. (B) and (C) Vegetation dieback expansion in Peel River tributaries Lomond Creek and KM99 stream is visible from expansion of dark areas in false color composites of satellite imagery of surface reflectance.

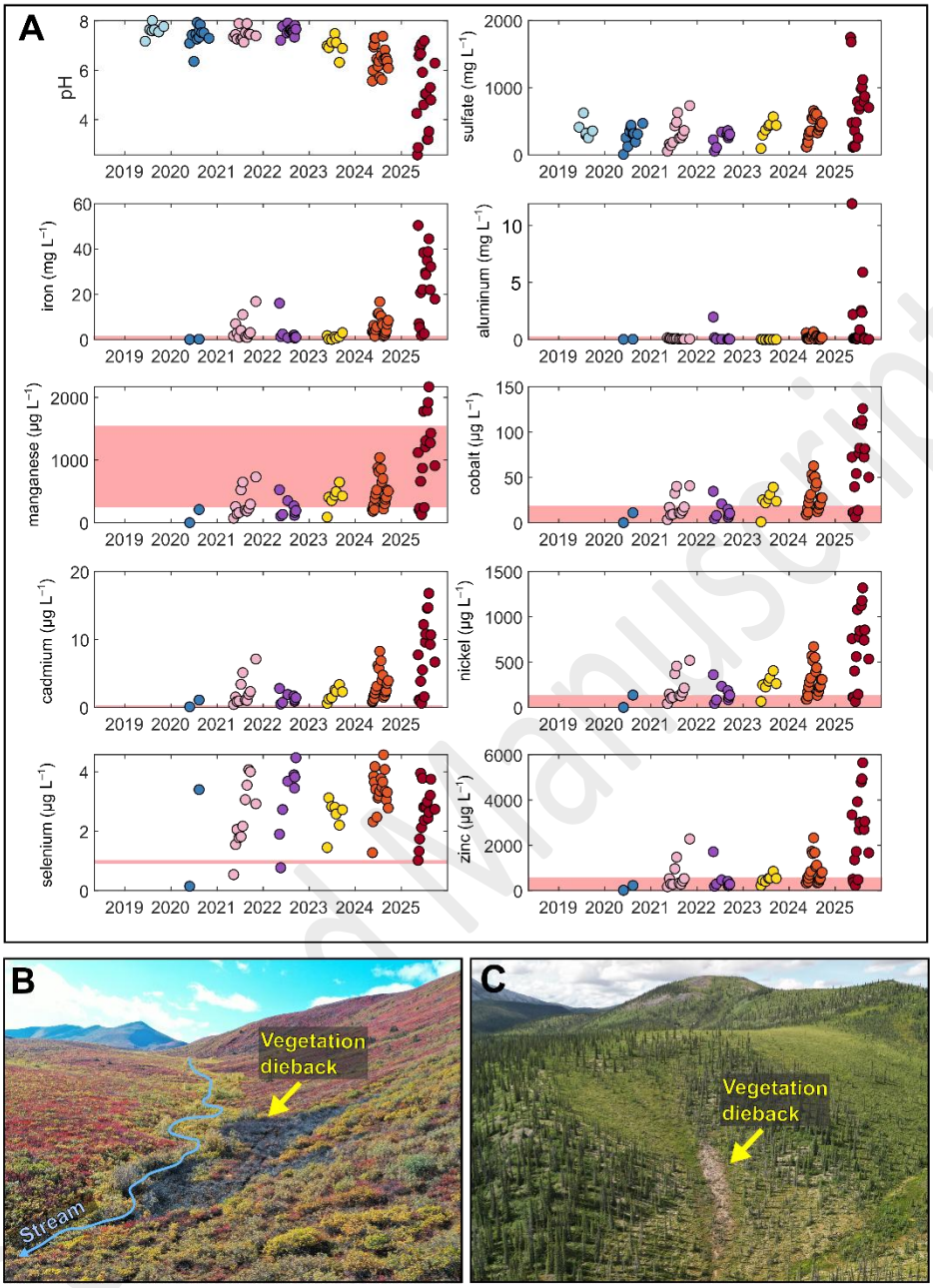

Fig. 2. Recent degradation of water quality from SMO intensification in headwater streams. (**A**) Increasing interannual metal and sulfate concentrations and decreasing pH in a headwater stream of the Tombstone Waters Observatory (KM175 stream, Mackenzie River basin). Red shading shows the range in Canadian guidelines for the protection of aquatic life for metals, where applicable, which vary with water chemistry (pH, hardness, and dissolved organic carbon content) depending on the metal. (B) Acid inputs occur in areas of vegetation dieback containing pH ~3 seepages in KM99 stream and (C) KM175 stream. Dieback areas are ~1,900 m^2 in panel B and ~2,000 m^2 in panel C.

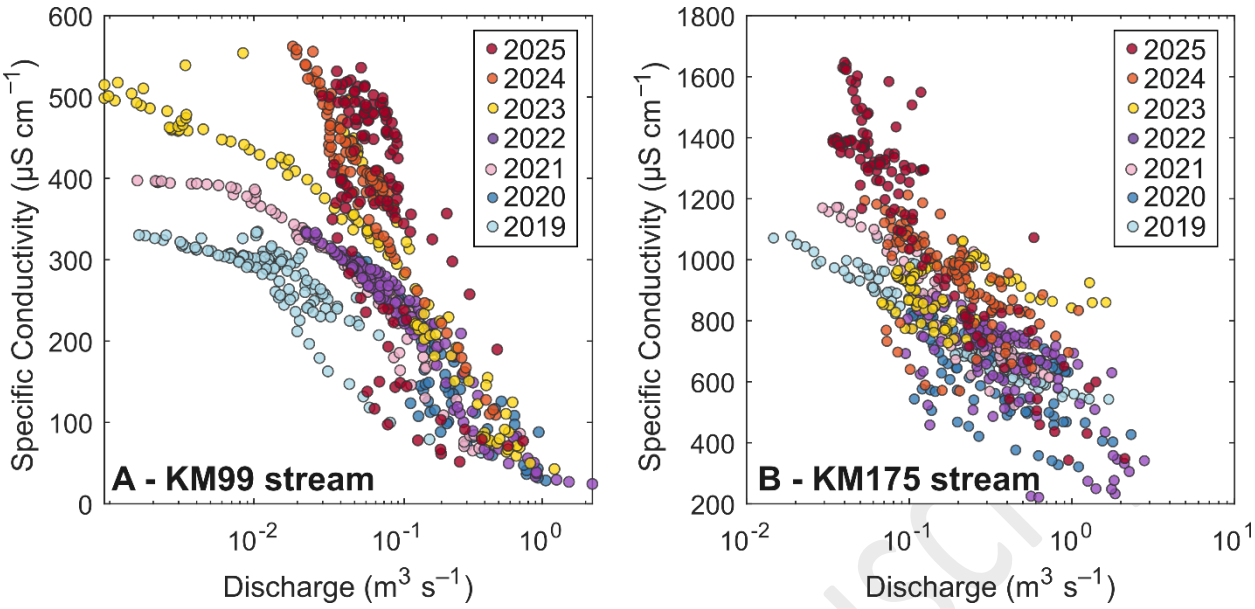

Fig. 3. Rising interannual specific conductivity from intensified SMO in headwater streams. Specific conductivity – discharge relationships show a stepwise interannual increase in specific conductivity beginning in 2023 and 2024 in Tombstone Waters Observatory streams of the Peel River basin. (A) KM99 stream. (B) KM175 stream.

5

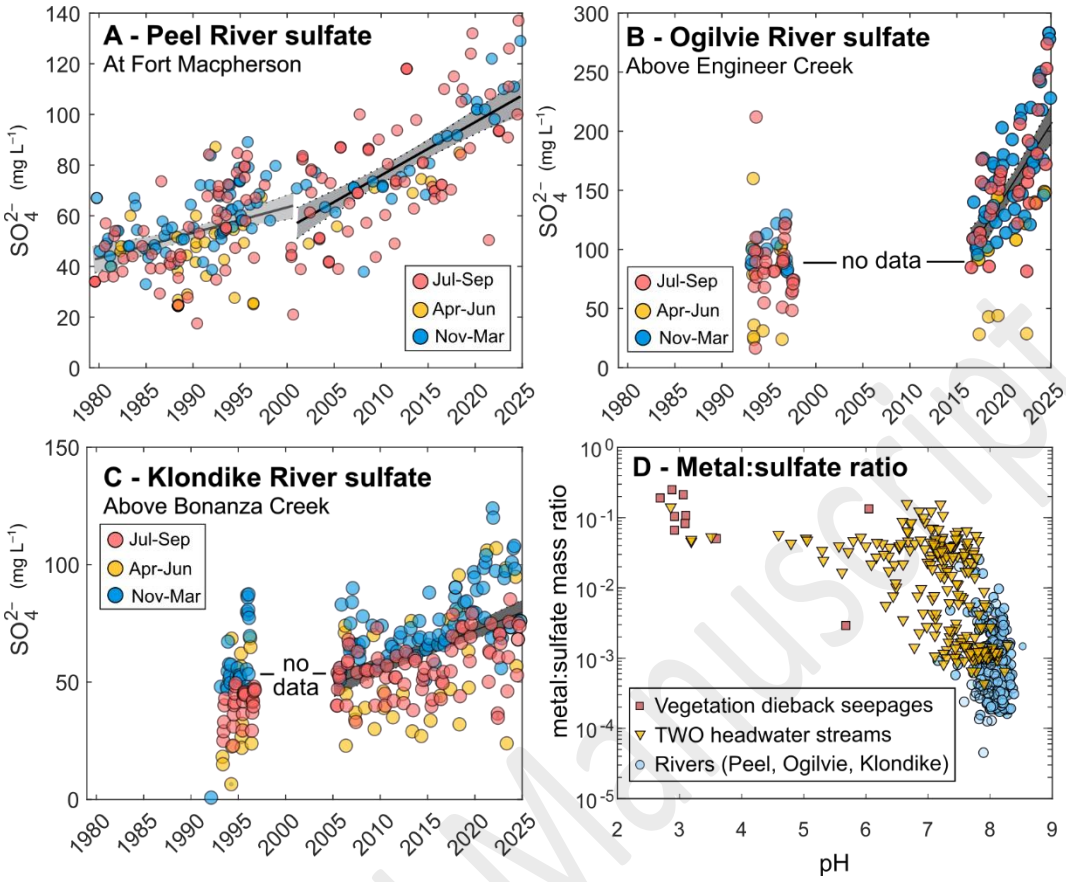

Fig. 4. Recent interdecadal rises of riverine sulfate concentrations from intensified SMO in the Mackenzie and Yukon river basins. Significant rises in sulfate concentrations have occurred in major tributary rivers of the Mackenzie and Yukon rivers downstream of the Tombstone Waters Observatory in recent decades because of intensified sulfide-mineral oxidation (A – Peel River; B – Ogilvie River; C – Klondike River). River water sulfate data symbols are grouped by season. Filter-passing metal export is modulated by pH-driven precipitation and sorption processes causing a decrease in metal/sulfate ratios from point-source acidic seepages to receiving headwater streams and large rivers (D).